HHS Public Access

Author manuscript

Nature. Author manuscript; available in PMC 2021 June 09.

Published in final edited form as:

Nature. 2020 August ; 584(7822): 614–618. doi:10.1038/s41586-020-2443-1.

Clinical targeting of HIV capsid protein with a long-acting small molecule

A full list of authors and affiliations appears at the end of the article.

Abstract

Oral antiretrovirals provide life-saving treatments for millions of people living with HIV (PLWH) and can prevent new infections via pre-exposure prophylaxis (PrEP)[1-5]. However, some heavily treatment experienced (HTE) PLWH have limited or no treatment options due to multi-drug resistance[6]. In addition, suboptimal adherence to oral daily regimens can negatively impact the outcome of treatment, contributing to virologic failure, resistance generation, and viral transmission, and of PrEP, leading to new infections[1,2,4,7-9]. Long-acting agents from new antiretroviral classes can provide much needed treatment options for HTE PLWH and additionally improve adherence[10]. Here we describe GS-6207, a small molecule that disrupts HIV capsid protein (CA) functions and is amenable to long-acting therapy due to its high potency, low in vivo systemic clearance, and slow subcutaneous injection-site release kinetics. With the benefit of X-ray crystallographic information, we designed GS-6207 to bind tightly at a conserved interface

*Correspondence and requests for materials should be addressed to stephen.yant@gilead.com.

Author contributions: T.C. conceived the project. D.J., M.H., and N.N. conducted protein purifications and X.L. and R.S. oversaw the analysis. S.R.Y., N.P., T.Z.C., D.K., and L.L designed, conducted and analyzed small molecule library screens. T.C., J.O.L., S.R.Y., R.L.H., W.C.T., M.S.R., and A.E.C. provided project leadership. J.O.L., W.C.T., S.D.S., C.-H.C., E.C., G.B., J.R.Z., J.L., M.G., P.M., Q.L., Q.W., R.L.H., R.D.S., S.D.S., S.E.L., and S.B. were responsible for the design, synthesis, characterization, and scale-up of small molecules. A. N.-M. conducted and analyzed in vitro CA assembly assays. S.R.Y. and A.N.-M. conducted and analyzed virion morphology by electron microscopy. G.J.S., S.A., and H.Y. designed, conducted and analyzed high-throughput antiviral measurements. G.J.S, S.A., A.M., and Y.X. conducted cell-based assays for cytotoxicity. G.J.S. conducted and analyzed in vitro drug combination studies. A.M. and R.R.R. conducted and analyzed in vitro antiviral testing against HIV mutants with resistance to existing agents. A.G.V. and R.L.A. conducted protein crystallization studies, J.R.S. collected and analyzed X-ray crystallographic data, and T.C.A. prepared the refinement table. C.E.C. and E.Y.H. conducted structural modeling studies to guide small molecule development. G.A.P., M.H.W., S.A.L., S.C., and L.L. conducted and analyzed biosensor binding studies. S.R.Y. A.M., E.S., and L.K.T. conducted and analyzed cell-based mechanism of action studies. A.L. conducted and analyzed biochemical protease assays. A.M., D.H., R.A.B., and S.R.Y. conducted resistance selection assays and characterized emergent HIV-1 CA variants. J.Z., B.L., and J.M. designed and executed preclinical PK and metabolism studies and summarized results. A.E.C. oversaw all anatomic pathology examinations and analyses of preclinical animal species. W.R., S.S., and A.C. designed and tested drug formulations. A.C. and S.A.W. oversaw GS-6207 chemistry, manufacture and control for clinical studies. M.S.R., R.H., R.B., and D.M.B. designed and supervised the clinical studies, and G.I.S., P.J.R., G.E.C., C.K.M., and E.S.D conducted them. R.B., J.L., Y.-P. L., N.M., and C.C. conducted and coordinated clinical sample and statistical analyses. W.I.S. provided project guidance during the early discovery phase and S.S. and W.E.L. provided long-term project oversight. S.R.Y., M.S.R., J.O.L., and T.C. wrote the manuscript, with input from all authors.

Competing interests: All authors are current or previous employees of Gilead Sciences (except G.I.S., P.J.R., G.E.C., C.K.M., W.I.S. and E.S.D.) and received salary and stock ownership as compensation for their employment. M.G., J.O.L., W.R., R.D.S., S.D.S., W.C.T., and J.R.Z. are inventors on granted US Patent No. 10,071,985B2 covering GS-6207 composition of matter and methods of use. G.I.S. receives research support from Gilead Sciences, Janssen Pharmaceutica, GlaxoSmithKline, Abbvie and Cepheid, and is on the speaker's bureau and advisory board for Janssen, ViiV Healthcare and Merck. G.E.C. receives grants (investigator research payments) from Gilead Sciences, ViiV Healthcare, Merck, and Janssen Pharmaceutica. C.K.M. receives research support from Gilead Sciences, Merck, ViiV Healthcare, and Jansen Pharmaceutica, is on the speaker's bureau for Gilead Sciences, Merck and Insmed, and is on an advisory board for Gilead Sciences. E.S.D. receives research support from Gilead Sciences, Merck and ViiV Healthcare and has served as a consultant for Gilead Sciences.

Additional Information: Supplementary Information is linked to the online version of the paper at www.nature.com/nature.

The authors declare competing interests: details are available in the online version of the paper. Further information on research design is available in the Nature Research Reporting Summary linked to this article.

between CA monomers, where it interferes with CA-mediated protein-protein interactions essential for multiple phases of the viral replication cycle. GS-6207 exhibits picomolar antiviral activity against all HIV-1 subtypes tested and shows high synergy and no cross-resistance with approved antiretroviral drugs. In Phase 1 clinical studies, monotherapy with a single subcutaneous dose of GS-6207 (450 mg) produced a mean 2.2 $\log_{10}$ plasma viral load reduction after 9 days and showed sustained plasma exposure at antivirally active concentrations for > 6 months. These results provide clinical validation for targeting HIV CA functions and demonstrate the potential of GS-6207 as a new long-acting agent to treat or prevent HIV infection.

HIV-1 CA protein (p24) has essential roles throughout the viral replication cycle, making it an attractive target for therapeutic intervention[11,12]. Unlike the viral enzymes currently targeted by small molecule antiretroviral drugs (protease (PR), reverse transcriptase (RT) and integrase (IN)), CA functions through protein-protein interactions, and such targets have historically posed significant challenges for small molecule drug intervention[13]. CA is initially expressed within the Gag and Gag-Pol polyproteins and provides key protein-protein interactions necessary for virion assembly[14]. In the virion, CA is released by PR-mediated precursor cleavage and self-assembles into a conical capsid composed of ~ 250 CA hexamers and 12 pentamers[15]. Proper capsid formation and integrity are essential for virus infectivity[14]. Upon infection of a new cell, controlled intracellular transport and disassembly of the viral capsid is regulated in part by interactions with host factors, and supports reverse transcription and proviral DNA integration[16-18].

We assayed small molecules for effects on the kinetics of in vitro CA assembly and identified multiple inhibitor and accelerator series. Potency improvements through chemical modification were limited for compounds that inhibited CA assembly, presumably because they could not overcome mass-action and CA subunit excess in the virion (~4 mM in the virion)[19,20]. Compounds that worked in concert with mass-action to increase the rate and extent of CA assembly proved more amenable to improvement of antiviral activity. Ultimately, extensive potency and pharmacokinetic optimization was required to discover a clinical candidate directed against this protein-protein interaction target. We previously reported on the activity of GS-CA1[21]. Here we report on GS-6207 (Fig. 1a), an even more potent and more metabolically stable CA-targeting inhibitor of HIV replication that is suitable for clinical trials[22]. GS-6207 showed a dose-dependent increase in the rate and extent of in vitro capsid assembly (Fig. 1b). In a cellular context, this acceleration of CA assembly produced malformed capsids that are morphologically distinct from mature and immature particles (Fig. 1c, d). Importantly, GS-6207 showed a mean half-maximum effective concentrations (EC_{50}) of 105 pM in HIV-1-infected MT-4 cells, making it significantly more potent than all approved HIV antiretroviral drugs tested (Fig. 1e). GS-6207 showed picomolar mean EC_{50} values in HIV-1-infected primary human $CD4^+$ T cells (32 pM) and macrophages (56 pM), and remained broadly active against two HIV-2 isolates (885 pM) and twenty-three clinical HIV-1 isolates (50 pM, range of 20 to 160 pM) in human peripheral blood mononuclear cells (PBMCs) (Fig. 1f). GS-6207 exhibited minimal cytotoxicity in human cell lines and primary cells with a mean half-maximal cytotoxic concentration (CC_{50}) in PBMCs of > 50 μM and a therapeutic index (CC_{50}/EC_{50}) of >1,000,000 (Extended Data Table 1). When combined with other antiretrovirals, GS-6207

displayed synergy (Extended Data Table 2) and retained full activity against HIV-1 variants resistant to current drug classes (Extended Data Table 3), demonstrating its potency in combination, and against drug-resistant HIV strains.

The molecular underpinnings for the role of GS-6207 as an accelerator of CA monomer assembly are apparent in a 2.0 Å resolution X-ray crystal structure of GS-6207 in complex with a cross-linked CA hexamer (Fig. 1g-i) (Extended Data Table 4). In this structure, GS-6207 binding is located between the N-terminal domain of one CA hexamer subunit (CA_{NTD}) and the C-terminal domain (CA_{CTD}) of an adjacent subunit in the hexamer. GS-6207 exhibits striking shape complementarity with adjacent CA monomers (contacting > 2,000 $Å^2$ of buried protein surface area) and displays extensive hydrophobic and electrostatic interactions including two cation-**π** interactions and seven H-bonds. The GS-6207 sulfonamide is the linchpin in a H-bonding network that bridges from CA_{NTD} residues N74 and K70 of one subunit to CA_{CTD} residue N183 of the neighboring subunit and orders a loop that is unstructured in the apo hexamer crystal (Fig. 1i). In accordance with its binding position between neighboring CA monomers in this crystal structure, GS-6207 showed saturable dose-dependent binding to Gag and CA, and its slow dissociation from CA multimers is consistent with a tenfold higher affinity relative to the CA monomer (Extended Data Table 5).

To define the functional consequences of GS-6207 binding to capsid, we measured the potency of GS-6207 during the early (in target MT-2 cells) and late (in producer HEK293T cells) stages of the viral replication cycle. GS-6207 showed subnanomolar potency in target cells (EC_{50} = 23 pM), in a full-cycle assay (EC_{50} = 25 pM), and in producer cells (EC_{50} = 439 pM), indicating that GS-6207 interferes with both the early and late stages of HIV-1 replication, but exhibits greater potency against the early stage (Fig. 2a). Time-of-addition studies relative to a non-nucleoside RT inhibitor and an IN strand transfer inhibitor indicated that GS-6207 targets one or more steps that occur after reverse transcription and prior to integration (Fig. 2b). In quantitative PCR assays, we measured the accumulation of the products of reverse transcription, 2-LTR circle formation (indicating nuclear localization but aborted integration), and proviral integration (Fig. 2c). GS-6207 at 1.25 nM (12.5-fold EC_{50}) did not alter HIV cDNA synthesis but significantly reduced formation of 2-LTR circles and integrated proviruses, suggesting that GS-6207 might prevent the nuclear import of viral cDNA, possibly via direct competition with capsid-binding host nuclear import co-factors that share the CA binding site with GS-6207, such as nucleoporin 153 (Nup153) and cleavage and polyadenylation specificity factor 6 (CPSF6)[23-26] (Fig. 2d). In addition to these early effects and the effects on capsid formation described above, GS-6207 also inhibited the production of HIV-1 containing mature wild-type CA, but not the CA M66I binding site mutant that reduces GS-6207 binding affinity to CA oligomers (Extended Data Table 5), as measured by p24 ELISA (Fig. 2e). GS-6207 did not inhibit HIV-1 PR cleavage activity in vitro (IC_{50} > 50 μM) but reduced intracellular Gag and processed CA levels in the producer cells (Fig. 2f), indicating that the loss of p24 production likely reflected GS-6207 binding to CA precursors and a reduction in Gag and/or Gag-Pol stability, trafficking and/or viral assembly.

To evaluate drug resistance, HIV-1 was serially passaged in MT-2 cells in the presence of increasing GS-6207 concentrations for > 3 months (Fig. 3a). Sequence analysis identified an N74D substitution in CA (passages 4-6) followed by a CA Q67H+N74D variant (passages 7-10). The N74D mutation has previously been shown to alter the viral pathway of nuclear entry[27]. Viruses with these GS-6207 resistance-associated mutations (RAMs) remained fully sensitive to other ARV classes (Fig. 3b). Selections performed in the presence of fixed concentrations of GS-6207 in human PBMCs independently infected with six HIV-1 isolates similarly identified Q67H and N74D as the major RAMs, with additional variants (L56I, M66I, K70N, Q67H+N74S and Q67H+T107N) each independently detected in a single GS-6207-selected culture (Fig. 3c). These RAMs, alone or in combination, conferred reduced susceptibility to GS-6207 (6- to >3,200-fold resistance relative to wild-type virus), consistent with the assignment of CA as the functional GS-6207 target. All residues conferring resistance map to the GS-6207 binding site and are highly conserved across HIV-1 subtypes[21,28-30]. Of the mutants tested, all but the low-level resistant Q67H variant (6-fold resistance to GS-6207) display reduced replication capacity in vitro (Extended Data Table 6).

Low hepatic clearance is an essential attribute for a long-acting agent. Thus, along with enhancement of potency, the design process culminating in GS-6207 was focused on blocking metabolically labile sites through incorporation of electron-withdrawing groups (halogens, sulfonyls), metabolically stable ring systems (cyclopropane, pyrazoles) and rigidifying elements. Tritiation [^{3}H] of GS-6207 was necessary to accurately measure its low turnover in primary human hepatocytes and showed a predicted rate of hepatic clearance of 0.01 L/h/kg, or 0.8% of the hepatic extraction.

In a randomized, double-blind, placebo-controlled, single ascending dose clinical study, a suspension formulation of 30 to 450 mg GS-6207 was administered to healthy participants (32 active vs. 8 placebo), who were mostly male (27 of 40) in their 30’s (median age: 37 years [range: 19 to 44]) with normal kidney and liver function as a subcutaneous injection (Fig. 4a). Consistent with nonclinical safety studies, GS-6207 was generally safe and well tolerated. The most frequent adverse events (AE) were mild injection site erythema or pain that resolved in a few days (Extended Data Table 7). GS-6207 pharmacokinetic profiles showed slow sustained drug release, with a median apparent terminal $t_{1/2}$ of ~38 days. Increases in GS-6207 exposure were approximately dose proportional. At doses ≥ 100 mg, GS-6207 plasma concentrations exceeded the human serum protein-adjusted 95% effective concentration ($paEC_{95}$) for wild-type HIV-1 (4.0 nM or 3.87 ng ml^{-1} in MT-4 cells) for ≥ 12 weeks, and doses ≥ 300 mg exceeded the human $paEC_{95}$ for > 24 weeks.

In a subsequent randomized, double-blind, placebo-controlled clinical study, 20 to 450 mg GS-6207 was administered to trial participants with untreated HIV-1 infection (24 active vs. 8 placebo) as a single dose subcutaneous suspension. We conducted a pre-specified interim analysis of this part of the study (Part A). Participants were mostly male (30 of 32) in their 30’s (median age: 34 years [range: 19 to 59]) who were treatment naïve (25 of 32) with median HIV-1 RNA loads of 4.48 $\log_{10}$ copies ml^{-1} (range: 3.86 to 5.01) and median CD4$^+$ T cell counts of 458 cells μl^{-1} (range: 200 to 1009). GS-6207 was generally safe and well tolerated (Extended Data Table 8), and its concentration-time profiles were consistent with

those in HIV-negative participants through 9 days post dose (Fig. 4b) (Extended Data Table 9). A single 20, 50, 150, or 450 mg subcutaneous administration of GS-6207 led to mean maximum 1.35, 1.79, 1.76, and 2.20 $\log_{10}$ reductions, respectively, in plasma HIV-1 RNA through 9 days (Fig. 4c) (Extended Data Table 10). A genetic mixture of wild-type and mutant capsid (Q67Q/H) emerged on day 9 in one participant in the 20 mg cohort, which was associated with a 1.6-fold decrease in phenotypic susceptibility, but not with viral escape through 9 days of monotherapy.

These data establish GS-6207 as a first-in-class HIV-1 capsid inhibitor with uniquely potent antiviral activity against both wild-type virus and variants resistant to current antiretrovirals. The favorable safety profile, prolonged pharmacokinetic exposure, and observed antiviral efficacy in humans support continued clinical development of GS-6207 as a novel long-acting antiretroviral agent for the treatment of HIV-1 infection, including HTE PLWH with multi-drug resistant virus. In addition, the infrequent subcutaneous dosing makes GS-6207 an attractive candidate for simplified prevention of HIV acquisition in at-risk populations as a potentially transformative tool in efforts to end the global HIV epidemic.

Methods

Compounds.

GS-6207 was synthesized at Gilead Sciences, and chemical identity (^{1}H-NMR, ^{13}C-NMR and high-resolution mass-spectrometry spectra) and sample purity were established using reverse phase HPLC (Supplementary Information). Control ARVs emtricitabine (FTC), tenofovir alafenamide (TAF), elvitegravir (EVG), raltegravir (RAL), bictegravir (BIC), darunavir (DRV), atazanavir (ATV) and bevirimat (BVM) were synthesized at Gilead Sciences, whereas efavirenz (EFV) and dolutegravir (DTG) were purchased from Toronto Research Chemicals and Porton Shanghai R&D Center, respectively. Puromycin (a control compound for cytotoxicity assays) was purchased from Sigma-Aldrich.

Viruses.

HIV-1_{IIIB} and HIV-1_{BaL} were obtained from the NIH AIDS Reagent Program and from Advanced Biotechnologies, respectively. Two HIV-2 isolates (CBL20, CDC310319) and 23 clinical HIV-1 isolates from the Southern Research virus collection were selected for susceptibility profiling: subtype A (92UG031, 92UG037), subtype B (89BZ_167, 90US_873, YU-2, 91US001, 91US004, 96TH_NP1538, BaL, JR-CSF), subtype C (92BR025, 98US_MSC5016), subtype D (92UG001, 98UG_57128), subtype E (CMU02, CMU08), subtype F (93BR020), subtype G (JV1083), Group N (YBF30), Group O (BCF01), CRF01_AE (90TH_CM235), and CRF02_AG (01CM0008BBY, 91DJ263). HIV-1 recombinant strains encoding mutation(s) conferring resistance to NRTIs, NNRTIs, INSTIs, PIs or MIs have been previously described[31,32]. Single-cycle HIV-1 encoding firefly luciferase with and without mutations within the capsid gene was made by co-transfecting HEK293T cells with pKS13ΔEnv and pHCMV-G plasmids. Cell-free viral supernatant was collected 3 days post-transfection, clarified using a 0.45 μm syringe filter and stored at −80°C. The amount of HIV in each sample was quantified by p24 antigen ELISA (Perkin Elmer) and a reverse transcriptase (RT) activity assay (Southern Research).

Cell lines.

Human MT-2 and MT-4 T-cell lines were obtained from the NIH AIDS Reagent Program and maintained in RPMI-1640 medium supplemented with 10% heat-inactivated fetal bovine serum (FBS), 100 units ml^{-1} penicillin, and 10 μg ml^{-1} streptomycin (complete RPMI). MT-2 cells chronically infected with $HIV\text{-}1_{IIIB}$ (MT-2/IIIB) were cultured in complete RPMI. HEK293T cells were obtained from the Gladstone Institute for Virology and Immunology and maintained in Dulbecco's modified Eagle's medium (DMEM) supplemented with 10% FBS, 100 units ml^{-1} penicillin, and 10 μg ml^{-1} streptomycin (complete DMEM). The human hepatoma Huh-7 cell line was obtained from ReBLikon GmbH and cultured in complete DMEM[33]. The human hepatoblastoma cell line HepG2, human prostate carcinoma cell line PC-3, and normal human fetal lung derived MRC-5 cells were obtained from the American Type Culture Collection. PC-3 and HepG2 cells were adapted to grow in 0.2% galactose-containing, glucose-free DMEM supplemented with 10% FBS, 1% non-essential amino acids, 1% Pyruvate, and 1% GlutaMAX. MRC-5 cells were maintained in Eagle's Minimum Essential Medium (MEM) supplemented with 10% FBS. Each cell culture medium was further supplemented with 100 units ml^{-1} penicillin and 100 μg ml^{-1} streptomycin. The above eukaryotic cell lines were not authenticated and were judged to be free of mycoplasma contamination using the MycoProbe Mycoplasma Detection Kit (R&D Systems).

Primary cells.

Human PBMCs were collected from healthy volunteers under informed consent; their use was approved by an institutional review board at AllCells. The preparation of human PBMCs, $CD4^+$ T-lymphocytes, and monocyte-derived macrophage cultures have been previously described[31]. Prior to infection, PBMCs and $CD4^+$ T-cells were activated for 48 h at 37°C by addition of 1 μg ml^{-1} phytohemagglutinin (PHA) and 50 international units ml^{-1} recombinant human interleukin-2 (IL-2). Primary human hepatocytes from three independent donors were purchased from Invitrogen and cultured in William's Medium E medium containing cell maintenance supplement. Donor profiles were limited to 4 – 65 years of age nonsmokers with limited alcohol consumption. Upon arrival at Gilead Sciences, hepatocytes were allowed to recover in a 37°C incubator with 5% CO_2 and 90% humidity for 12 – 18 h in complete medium with vendor-supplied supplements before treatment with compounds.

Antiviral assays.

The 5-day cytoprotection antiviral assays using MT-2 and MT-4 T-cell lines have been previously described[31]. Data analysis was performed using GraphPad Prism 7.0 to calculate EC_{50} values. The EC_{95} value for GS-6207 was calculated from the EC_{50} and Hill coefficient, n, determined in MT-4 cells using the equation: $EC_{95} = EC_{50} \times (95/5)^{1/n}$.

For time-of-addition antiviral assays, MT-2 cells were infected with single-cycle reporter HIV-1 for 1 h at 37°C, washed, and seeded into 96-well plates (75 μl aliquots; 1.5×10^4 cells per well). A 25 μl aliquot of complete RPMI media was added to 8 uninfected and 8 infected wells as respective minimum (0%) and maximal (100%) infection controls. Twenty-five μl aliquots of 4x drug-media were added to 8 replicate wells at indicated times post-infection.

GS-6207 and control ARVs were tested at concentrations equivalent to 10x and 100x EC_{50}, producing similar results. Assay plates were kept in a humidified 37°C incubator before and after drug-media additions. Plates were developed 48 h post-infection (h.p.i.) using ONE-Glo Luciferase Assay reagent (Promega) and the resulting luminescence data collected and analyzed using EnVision Manager 1.13.3009 and GraphPad Prism 7.0 softwares, respectively. When interrogating inhibitor potency across the phases of viral replication, single-cycle antiviral assays were performed in MT-2 cells in a manner such that GS-6207 was present selectively at early stage, late stage, or during a full course of infection as previously described[34]. Assays evaluating the effect of GS-6207 on HIV-1 particle production (by p24 antigen ELISA) and intracellular CA levels (by anti-p24 and anti-tubulin Western blot analyses) have been previously described[21].

For *in vitro* two-drug combination studies, compounds within a test pair were combined in 384-well assay plates to create a two-dimensional matrix of diluted drugs. Positive control (EVG) and negative control (dimethyl sulfoxide, DMSO) wells were included in every assay plate to define 100% and 0% protection from viral replication-mediated cytopathic effect (CPE), respectively. The final DMSO concentration in the assay was 0.5%. MT-2 cells were bulk infected in complete RPMI media with HIV-1_{IIIB} at a multiplicity-of-infection (m.o.i.) of 0.01 for 3 h at 37°C, added to the assay plates (3×10^3 cells per well) and incubated at 37°C for 5 days. Cell viability was determined by adding CellTiter-Glo reagent and the resulting luminescence data collected using EnVision Manager 1.13.3009. Data were normalized to positive and negative controls in each plate, expressed as % CPE protection, and analyzed with the MacSynergy II software[35]. Combination data were analyzed at the 95% confidence level, with synergy/antagonism volumes defined as follows: high synergy (>100 μM^2%), moderate synergy (50 to <100 uM^2%), additivity (>−50 to <50 μM^2%), and antagonism (<−50 μM^2%).

Antiviral assays using HIV-1_{BaL} in primary human $CD4_+$ T-lymphocytes and macrophage cultures were conducted using a p24 endpoint assay as previously described[36]. A 7-day reverse transcriptase (RT) endpoint antiviral assay using fresh human PBMCs independently infected with a panel of clinical HIV-1 and HIV-2 isolates was performed by Southern Research as a contracted research study.

Cytotoxicity assays.

For cytotoxicity assessment in MT-4 cells, PBMCs, primary human $CD4^+$ T-cells and monocyte-derived macrophages, the protocol was identical to that of the respective antiviral assay, including assay duration, except that no virus was added to the plates. Protocols for cytotoxicity assessments in Huh-7, Gal-HepG2, Gal-PC-3 and MRC-5 cell lines, as well as in primary human hepatocytes, have been previously described[37]. The effect of test compounds on cell viability was measured using CellTiter-Glo. Data analysis was performed using GraphPad Prism 7.0 to calculate CC_{50} values.

GS-6207 resistance analysis.

Dose-escalation selections for drug-resistant HIV-1 variants were performed in MT-2 cells infected with HIV-1_{HXB2D} using twofold incremental increases in GS-6207 concentration as

previously described[31]. The resistance profile of each emergent virus passage was then assessed in the 5-day cytoprotection antiviral MT-2 assay after titrating virus inoculums to normalize the m.o.i. across all samples. Viral breakthrough selections were conducted under conditions of fixed, constant drug concentrations over a period of 35 days in human PBMCs independently infected with six different HIV-1 isolates (BaL, 92US657, 91US0006, 7406, 7467 and 7576) as previously described[21]. GS-6207 was tested at fixed drug concentrations equal to 4-fold, 8-fold, and 16-fold its EC_{95} value of 0.23 nM (0.92 nM, 1.9 nM, and 3.7 nM GS-6207, respectively), using six replicate cell cultures per experimental condition. Viruses that emerged in the presence of GS-6207 were genotyped by population sequencing. Total RNA was isolated from mock- and GS-6207-selected virus-containing supernatants using the QiaAMP Viral RNA Mini Kit (Qiagen). A 986-bp fragment encoding HIV-1 capsid and the adjacent p2 spacer peptide was amplified by RT-PCR using the Qiagen OneStep RT-PCR Kit in combination with primers 5'-CAGTAGCAACCCTCTATTGTGTGC-3' and 5'-CCTAGGGGCCCTGCAATTT-3'. RT-PCR products were sequenced by Elim Biopharmaceuticals. To identify codon changes, gene sequences from selected HIV-1 variants were aligned using DNA Sequencher 4.9 Software (Gene Codes Corporation) with that of the input virus and virus passaged in the absence of GS-6207. For samples containing > 1 codon change, PCR products were subcloned, DNA was isolated from individual bacterial colonies, and the CA gene was sequenced to assess the linkage of all observed substitutions.

The resistance profile and infectivity of each GS-6207-selected CA variant was determined in MT-2 cells after introducing each substitution, alone and in combination, into wild-type single-cycle reporter HIV-1. The replication level (fitness) of select CA variants introduced into wild-type replication-competent reporter HIV-1 was evaluated in primary human $CD4^+$ T cells over a period of 19 days[21].

Recombinant HIV-1 Gag and CA proteins.

Recombinant HIV-1_{LAI} CA protein was prepared as previously described[38]. Soluble cross-linked HIV-$1_{NL4.3}$ CA hexamers (WT and the M66I variant) and CA pentamers were prepared as previously described[38-40]. Recombinant HIV-$1_{NL4.3}$ Gag protein was prepared as previously described[21].

Crystallization, data collection and structure determination.

HIV-1 CA hexamer protein (25 mg ml^{-1} in 20 mM Tris, pH 8.0) was thawed and diluted to 12 mg ml^{-1} in the same buffer and incubated on ice for 10 min with 1 mM GS-6207. Crystallization droplets were assembled in MRC2 microplates with 100 nl of the complex and 100 nl of 12% polyethylene glycol (PEG) 3350, 0.2 M sodium thiocyanate, 0.1 M sodium cacodylate, pH 6.7. The assembled 200 nl droplet was then subjected to vapor diffusion with 50 μl of 1% PEG 3350, 0.2 M sodium thiocyanate, 0.1 M sodium cacodylate, pH 6.7 in the large reservoir. Large hexagonal crystals (30 μm x 160 μm x 160 μm) grew in 4 d at 25°C and were subsequently cryo-protected for X-ray diffraction in 30% PEG 3350, 7% glycerol, 0.2 M sodium thiocyanate, 0.1 M sodium cacodylate, pH 6.7, and 0.3 mM GS-6207. X-ray diffraction data to 2.0 Å resolution were collected on a single frozen (−180°C) crystal at the Advanced Light Source, Beamline 5.0.1 (Berkeley, CA). The

protein-inhibitor complex crystallized in space group P3 with cell parameters: a = 158.3 Å, b = 158.3 Å, c = 55.6 Å, α = 90.0°, β = 90.0°, and γ = 120.0°. The data were processed and scaled with the programs DENZO and SCALEPACK (HKL Research Inc., Charlottesville, VA), respectively. Initial models were obtained by molecular replacement using the program EPMR[41] and utilizing the coordinates from a single monomer of a previously determined HIV-1 capsid hexamer-inhibitor complex (with coordinates for the inhibitor atoms removed) as the search model. The molecular replacement solution included six monomers. The initial model was further refined using multiple rounds of simulated annealing in the PHENIX software package[42] followed by manual re-fitting of the model in COOT[43]. In the later stages of refinement, strong residual electron density in the capsid modulator binding site allowed for unambiguous placement of GS-6207 into the structure followed by final refinement of the model (see Supplementary Figure 2 for sample inhibitor density). Data collection and model refinement statistics are summarized in Extended Data Table 4.

In vitro HIV-1 CA assembly assay.

The in vitro assembly of HIV-1 CA protein in the presence and absence of small molecule library compounds (10 μM) or 2-fold serially diluted GS-6207 was monitored by measuring changes in sample absorbance over time at 350 nm. Final assembly reactions contained 20 μM CA, 2 M NaCl, 50 mM sodium phosphate pH 7.5, 0.005% Antifoam 204 (Sigma-Aldrich) and 1% DMSO. Sample absorbance values at 350 nm were monitored over time at 25°C in 96-well or 384-well plates using an M5 plate reader (Molecular Devices), corrected for absorbance values in the absence of CA or NaCl, and the data analyzed using SoftMax Pro 6.3.1 as previously described[38].

GS-6207 binding assay.

Surface plasmon resonance biosensor binding experiments were performed using the ProteOn XPR36 platform (CA hexamer and pentamer proteins) or the Biacore T100 platform (CA monomer and Gag proteins) as previously described[21]. Data were analyzed using ProteOn Manager 3.1.0 or Scrubber 2.0 and fit with a simple kinetic model with a term for mass transport added when necessary.

Quantitation of HIV-1 DNA.

MT-2 cells (2 x 10^6 cells ml^{-1}) were infected with single-cycle reporter HIV-1, added to 24-well plates, drug media and transferred to a humidified 37°C incubator. For each condition, cells from each of 3 replicate wells were harvested 12 h.p.i. for late RT product quantification, 24 h.p.i. for 2-LTR circle quantitation, and 48 h.p.i. for Alu-LTR product quantification. Viral DNA was isolated from cell pellets using a QIAamp DNA mini kit (Qiagen) and quantified using the TaqMan real-time PCR and ABI Prism 7900HT sequence detection system (Applied Biosystems) or the QX200 Droplet Digital PCR (ddPCR) System (Bio-Rad) as previously described[21].

Ultrastructural analysis of HIV-1 by electron microscopy.

MT-2/IIIB cells were washed and cultured at 37°C in complete RPMI containing 0.25% DMSO, 15 nM GS-6207 or 500 nM ATV. After a 4-day incubation, samples were pelleted,

fixed, stained, sectioned and imaged on a JEOL JEM-1230 transmission electron microscope as previously described[21].

Metabolic stability of [^{3}H]GS-6207 in primary human hepatocytes.

A 500 μl suspension of human hepatocytes (1×10^6 cells ml^{-1}) and 0.25 μM [^{3}H]GS-6207 was prepared in Krebs-Henseleit Buffer (KHB) medium and incubated in a humidified 37°C incubator with 5% CO_2 in duplicate wells of a 24-well plate. Propranolol (1 μM final), a compound known to be efficiently metabolized by hepatocytes by oxidation and conjugation, was used as a positive control. A cell-free control was incubated in parallel as a negative control. Aliquots (100 μl) were removed after 0, 1, 3, and 6 h, mixed with 200 μl quenching solution, placed on a shaker for 10 min and then centrifuged at 3000 × g for 60 min. The supernatant was transferred to a new plate, diluted with 100 μl water and placed on a shaker for 10 min. The quantification of [^{3}H]GS-6207 and its metabolites was performed by radio flow chromatography using a Perkin Elmer Radiomatic 625TR flow scintillation analyzer with a 500 μl flow cell coupled to a Dionex Ultimate® 3000 HPLC system. The scintillation cocktail was Perkin Elmer Ultima-Flo™ and was mixed with the HPLC effluent at a ratio of 1:1. The sample (100 μl) was injected with a Leap Technologies CTC PAL autosampler. Separation was achieved on a Phenomenex Synergi Fusion-RP 80 Å pore size, 4 μm particle size, 150 × 4.6 mm column maintained at 32°C. Mobile phase A consisted of 95% water, 5% acetonitrile, and contained 0.1% trifluoroacetic acid (TFA). Mobile phase B consisted of 95% acetonitrile, 5% water, and contained 0.1% TFA. Elution was achieved, at a flow rate of 1 ml min^{-1}, by linear gradients: initial condition was 2% B at 0 min which was increased to 75% B over 45 min, holding for 4 min at 75% B and then returning to initial conditions. The column was allowed to re-equilibrate for 12 min between injections. Quantification was by radiochromatographic peak area.

Competitive equilibrium dialysis.

Human serum protein binding to GS-6207 was determined by competitive equilibrium dialysis. Human plasma (10%) was spiked with GS-6207 (2 μM) and blank RPMI cell culture medium containing 2% FBS were placed in duplicate into opposite sides of assembled dialysis cells. After a 24-h equilibration period at 37°C, GS-6207 concentrations in plasma and cell culture medium were determined by a liquid chromatography tandem mass spectrometry (LC-MS/MS) method and multiplied by 10 to obtain the protein-adjusted shift for 100% human plasma.

Clinical trials: ethical conduct and consent.

The clinical trials were conducted in accordance with Good Clinical Practice, as defined by the International Conference on Harmonisation and in accordance with the ethical principles underlying the United States Code of Federal Regulations, Title 21, Part 50 (21CFR50). The protocol and the subject informed consent form received institutional review board/ independent ethics committee approval/favorable opinion (Advarra, Columbia, MD) before initiation of the study. Freely given written informed consent was obtained from every subject before participation in the clinical studies.

Clinical trials: single ascending-dose study in healthy participants.

For clinical Study GS-US-200-4070, we enrolled HIV-1-uninfected healthy men and women, 18-45 years of age, with normal kidney and liver function, body mass index between 19 and 30 kg/m^2, and no significant medical history. Ten trial participants in each dosing arm were randomized in a blinded fashion in a 4:1 ratio to receive either the drug (GS-6207) or placebo (vehicle alone). The primary objectives were to assess the safety and tolerability of escalating single subcutaneous doses of GS-6207 compared with placebo in healthy participants and to assess its pharmacokinetics (PK). GS-6207 was formulated as a sterile, preservative-free, injectable aqueous suspension (100 mg $m1^{-1}$). Serial blood samples were collected for plasma PK analysis through day 197 (30 and 100 mg Cohorts) or day 225 (300 and 450 mg Cohorts). Plasma samples were analyzed using a validated, high-performance LC-MS/MS bioanalytical method with multiple reaction monitoring (MRM) and electrospray ionization in the positive mode (Covance Laboratories). Quantification was performed using MRM of the transitions m/z 968.2 → 869.2 and m/z 974.3 → 875.2 for GS-6207 and an isotopically labeled internal standard, respectively. The bioanalytical method was validated over a calibrated range of 0.5 to 500 ng ml^{-1}. Inter assay precision, based on coefficient of variation, was ≤ 8.7%, and accuracy ranged from 95.2% to 104.6%. All plasma samples were analyzed within the timeframe supported by frozen stability storage data. Pharmacokinetic parameters were estimated using Phoenix® WinNonlin® 6.4 (Certara, L.P.) software using standard noncompartmental methods. PK parameters for GS-6207 included area under plasma concentration versus time curve extrapolated to infinity (AUC_{inf}), the percent of the area that is extrapolated ($AUC_{\%exp}$), and area under the concentration versus time curve from time zero to the last quantifiable concentration (AUC_{last}), maximal concentration (C_{max}), time to C_{max} (t_{max}), and half-life ($t_{1/2}$).

Clinical trials: single ascending-dose study in participants living with HIV.

For clinical Study GS-US-200-4072 (registered with ClinicalTrials.gov, NCT03739866), we enrolled treatment-naive or -experienced, but HIV capsid inhibitor naïve and integrase strand transfer inhibitor naïve, men and women, 18–65 years of age with plasma HIV-1 RNA ≥ 5,000 copies ml^{-1} (via amendment; originally 10,000 copies ml^{-1}) but ≤ 400,000 copies ml^{-1} and $CD4^+$ T cell counts > 200 cells/mm^3. Eight trial participants in each dosing arm were randomized in a 3:1 ratio to receive either the drug (GS-6207) or placebo (vehicle alone) (Part A). GS-6207 was formulated as a sterile, preservative-free, injectable aqueous suspension (100 mg $m1^{-1}$). Plasma HIV-1 RNA levels were determined using the Roche COBAS Ampliprep/COBAS TaqMan HIV-1 test v.2, which has a limit of detection of 20 copies ml^{-1} and a range of quantification of 20 to 10,000,000 HIV-1 RNA copies ml^{-1}. All samples were analyzed by a central laboratory. Serial blood samples were collected for plasma PK through at least day 9. PK samples were analyzed as above for Study 200-4070.

HIV-1 resistance analyses for Study GS-US-200-4072 were carried out at Monogram Biosciences using the research-grade gag-PR genotyping (population-level sequencing) and phenotyping assay to assess resistance to GS-6207 using participant's HIV-1 DNA fragment encompassing the gag-PR HIV-1 region, and/or using the CLIA-certified PhenoSense GT + Integrase® or GenoSure PRIme® assay to assess resistance to the components of Biktarvy® (which was administered to all participants following the 9-day GS-6207 monotherapy).

Resistance analyses were conducted at screening and Day 9 (last GS-6207 monotherapy visit). Within Part A, we conducted an interim analysis, which was pre-specified in the protocol to be conducted after at least 50% of the participants and/or after all participants within each cohort completed the Day 10 visit. The purpose of this interim analysis was to select the doses of GS-6207 to evaluate in each subsequent cohort.

Statistics.

GraphPad Prism 7.0 was used for statistical analysis. In each case, an unpaired two-tailed Student's t test with Welch's correction was performed for parametric analysis of two groups. A P value < 0.05 was considered statistically significant.

Data availability:

All data to understand and assess the conclusions of this research are available in the main text and Supplementary Information. Raw gel source data for Fig. 2f is available in Supplementary Figure 1. Small molecule X-ray crystallographic coordinates and structure factor files have been deposited in the Protein Data Bank (PDB, www.rcsb.org) with accession number 6V2F. Study GS-US-200-4072 was registered with ClinicalTrials.gov, NCT03739866. The datasets generated during and/or analyzed during the current study are available from the corresponding author on reasonable request.

Extended Data

Extended Data Table 1.

Cytotoxicity of GS-6207 in human cell lines and primary cells

	CC_{50} (μM)	
	GS-6207	**Puromycin**
Human cell lines		
MT-4	24.7 ± 18.3	0.2 ± 0.1
Huh-7	>44.4	0.5 ± 1.7
Gal-HepG2	>44.4	1.0 ± 1.7
Gal-PC-3	>44.4	0.4 ± 1.5
MRC-5	>44.4	0.3 ± 1.5
Human primary cells		
Hepatocytes	>50.0	1.6 ± 0.6
Quiescent PBMCs	>44.4	0.6 ± 1.5
Stimulated PBMCs	>50.0	0.2 ± 0.1
$CD4^+$ T-lymphocytes	>50.0	0.2 ± 0.1
Monocyte-derived macrophages	>50.0	4.5 ± 2.8

CC_{50}, half-maximal cytotoxic concentration; PBMCs, peripheral blood mononuclear cells. Data are mean ± s.d. from three independent experiments (n = 4 biological replicates each). Puromycin was assayed in parallel as a positive control for cytotoxicity.

Extended Data Table 2.

In vitro combination studies with GS-6207

	TAF	EFV	DTG	DRV	GS-6207
Synergy volume [μM^2.%]	87 ± 32	101 ± 40	116 ± 13	119 ± 39	18 ± 8
Antagonism volume [μM^2.%]	−8 ± 7	−8 ± 8	−8 ± 7	−3 ± 3	−16 ± 6
Combination effect	Moderately synergistic	Highly synergistic	Highly synergistic	Highly synergistic	Additive

TAF, tenofovir alafenamide (nucleotide reverse transcriptase inhibitor); EFV, efavirenz (nonnucleoside reverse transcriptase inhibitor); DTG, dolutegravir (integrase strand transfer inhibitor); DRV, darunavir (HIV protease inhibitor); GS-6207 in combination with itself was included as a positive control for additivity. Data are mean ± s.d. from three independent experiments (n = 3 biological replicates each). The high antagonism control combination of ribavirin and stavudine produced the expected results (synergy volume = 0 ± 0; antagonism volume = −398 ± 23).

Extended Data Table 3.

GS-6207 activity against HIV-1 isolates resistant to existing antiretroviral inhibitors

		Fold resistance (n)		
Antiretroviral Class	**HIV-1 Mutant**	**GS-6207**	**Control**	**Antiretroviral Agent**
Nucleotide reverse transcriptase inhibitor (NRTI)	K65R	0.6 ± 0.2 (3)	FTC	14.1 ± 2.6 (3)
	M184V	0.3 ± 0.3 (3)	FTC	>23.0 (3)
	6TAMs	0.2 ± 0.1 (3)	FTC	4.0 ± 2.8 (3)
Nonnucleoside reverse transcriptase inhibitor (NNRTI)	Y188L	0.5 ± 0.1 (3)	EFV	>22.5 (3)
	L100I+K103N	0.5 ± 0.2 (3)	EFV	>22.5 (3)
	K103N+Y181C	0.6 ± 0.2 (3)	EFV	>22.5 (3)
Integrase strand transfer inhibitor (INSTI)	E138K+Q148K	0.6 ± 0.3 (3)	EVG	>53.8 (3)
	G140S+Q148R	0.8 ± 0.3 (3)	EVG	>53.8 (3)
	E92Q+N155H	0.8 ± 0.4 (3)	EVG	>53.8 (3)
	N155H+Q148R	1.2 ± 0.7 (3)	EVG	>52.9 (3)
Maturation inhibitor (MI)	V230I in CA	0.7 ± 0.2 (6)	BVM	>67.5 (6)
	V7A in SP1	0.8 ± 0.4 (8)	BVM	>67.5 (7)
Protease inhibitor (PI)	M46I+I50V	0.7 ± 0.2 (3)	DRV	27.1 ± 23.1 (3)
	I84V+L90M	0.3 ± 0.1 (3)	ATV	32.7 ± 7.8 (3)
	G48V+V82A+L90M	0.5 ± 0.2 (3)	ATV	31.0 ± 11.9 (3)
	G48V+V82S	0.4 ± 0.2 (3)	ATV	15.2 ± 3.2 (3)

FTC, emtricitabine; EFV, efavirenz; EVG, elvitegravir; BVM, bevirimat; DRV, darunavir; ATV, atazanavir; SP1, 14-amino acid spacer peptide 1, located between CA and nucleocapsid (NC) in HIV-1 Gag; 6TAMs, six non-polymorphic HIV-1 RT mutations (M41L, D67N, K70R, L210W, T215Y and K219Q) that confer resistance to thymidine analogs. Data are geomean ± s.d. from three biological replicates in each of at least three independent experiments (exact n denoted in parentheses).

Extended Data Table 4.

Data collection and refinement statistics (molecular replacement)

	HIV-1 Capsid hexamer - GS-6207 complex
Data collection	
Space group	P3
Cell dimensions	
a, b, c (Å)	158.30, 158.30, 55.65
α, β, γ (°)	90, 90, 120
Resolution (Å)	30.00 - 2.00 (2.07 - 2.00) *
R_{sym} or R_{merge}	0.119 (0.795)
$I / \sigma I$	18.80 (1.94)
Completeness (%)	98.66 (90.82)
Redundancy	5.2 (4.3)
Refinement	
Resolution (Å)	29.18 - 2.00 (2.07 - 2.00)
No. reflections	105,864 (9,768)
R_{work} / R_{free}	0.2051 / 0.2492 (0.2447 / 0.2712)
No. atoms	
Protein	9,456
Ligand/ion	384
Water	896
B-factors	
Protein	30.72
Ligand/ion	25.60
Water	38.83
R.m.s. deviations	
Bond lengths (Å)	0.003
Bond angles (°)	0.570
Ramachandran statistics	
Favored (%)	99.40
Allowed (%)	0.60
Outliers (%)	0.00
Rotamer outliers	0.00

All data were collected from a single crystal.

*Values in parentheses are for highest-resolution shell. For inhibitor electron density defined by X-ray crystallography, see Supplementary Figure 2.

Extended Data Table 5.

Biosensor surface plasmon resonance assays of GS-6207 binding to recombinant CA

	Immature capsid	Mature capsid			
	Gag polyprotein	CA monomer	CA pentamer	CA hexamer	CA hexamer_M66I
K_D (pM)	1,100 ± 900	2,500 ± 500	220 ± 160	240 ± 90	60,000 ± 20,000
k_{on} ($M^{-1}s^{-1}$)	ND	ND	$2 \pm 1 \times 10^5$	$6.5 \pm 0.3 \times 10^4$	$6 \pm 4 \times 10^4$
k_{off} (s^{-1})	ND	ND	$2.7 \pm 0.4 \times 10^{-5}$	$1.4 \pm 0.4 \times 10^{-5}$	$2.6 \pm 0.3 \times 10^{-3}$

M66I is an in vitro GS-6207-selected CA binding site mutant that confers high-level resistance to GS-6207. ND, not determined because the binding rate was too fast to be determined reliably. Data are mean ± s.d. from four independent experiments (or three for the M66I variant) assayed in singlet.

Extended Data Table 6.

Resistance profile of HIV-1 CA mutants identified in viruses selected by GS-6207

HIV-1 CA Sequence	WT	Q67H	N74D	K70N	Q67H N74S	Q67H T107N	L56I	Q67H N74D	M66I
Mean EC_{50} (pM) in MT-2 cells [*]	31	196	682	741	996	1,910	7,400	34,069	>100,000
Fold GS-6207 resistance [†]	1	6	22	24	32	62	239	1,099	>3,226
Infectivity (% WT) in a single-cycle replication assay in MT-2 cells [‡]	100	95	48	7	34	41	9	29	6
Peak replication level (% WT) in primary human $CD4^+$ T-cells infected with a replication-competent reporter HIV-1 [§]	100	100	1	1	69	28	3	<1	<1

[*] Data are mean single-cycle EC_{50} values from three independent experiments (n = 3 biological replicates each).

[†] Data are mean mutant/wild-type (WT) EC_{50} ratios from three independent experiments (n = 3 biological replicates each).

[‡] Data are mean luminescence values expressed as a percentage of the WT virus from three independent experiments (n = 3 biological replicates each).

[§] Data are mean luminescence values expressed as a percentage of the WT virus from two independent experiments (n = 6 biological replicates each).

Extended Data Table 7.

Baseline characteristics and clinical adverse events in healthy participants (>1 participant overall) in study GS-US-200-4070

	GS-6207					
Baseline characteristics	30 mg (n = 8)	100 mg (n = 8)	300 mg (n = 8)	450 mg (n = 8)	Placebo (n = 8)	Overall (n = 40)
Age, years, median (range)	40 (29-43)	36 (19-42)	34 (22-41)	36 (27-42)	41 (21-44)	37 (19-44)
Sex at birth: female, n (%)	3 (38)	5 (63)	3 (38)	1 (13)	1 (13)	13 (33)
Race: black, n (%)	3 (38)	2 (25)	1 (13)	3 (38)	2 (25)	11 (28)
Body mass index, kg/m^2, median (range)	28 (23-30)	26 (21-29)	24 (23-30)	28 (23-30)	27 (21-30)	26 (21-30)
Safety: preferred term						
Any AE, n (%)	4 (50)	8 (100)	7 (88)	6 (75)	4 (50)	29 (73)

Baseline characteristics	GS-6207 30 mg (*n* = 8)	GS-6207 100 mg (*n* = 8)	GS-6207 300 mg (*n* = 8)	GS-6207 450 mg (*n* = 8)	Placebo (*n* = 8)	Overall (*n* = 40)
Injection site erythema	1 (13)	5 (63)	6 (75)	3 (38)	0	15 (38)
Injection site pain	0	3 (38)	6 (75)	3 (38)	2 (25)	14 (35)
Injection site nodule	0	5 (63)	3 (38)	1 (13)	0	9 (23)
Injection site induration	0	0	6 (75)	2 (25)	0	8 (20)
Injection site swelling	1 (13)	5 (63)	1 (13)	0	0	7 (18)
Headache	2 (25)	1 (13)	2 (25)	0	0	5 (13)
Injection site pruritus	1 (13)	0	1 (13)	1 (13)	0	3 (8)
Viral upper respiratory tract infection	0	0	0	2 (25)	1 (13)	3 (8)
Acne	0	0	0	2 (25)	0	2 (5)
Back pain	0	0	2 (25)	0	0	2 (5)
Dizziness	0	0	1 (13)	1 (13)	0	2 (5)
Injection site bruising	0	0	1 (13)	0	1 (13)	2 (5)
Nausea	1 (13)	0	1 (13)	0	0	2 (5)
Oropharyngeal pain	1 (13)	0	0	0	1 (13)	2 (5)
Skin mass	0	0	1 (13)	1 (13)	0	2 (5)

Extended Data Table 8.

Baseline characteristics and clinical serious adverse events (any) and adverse events (>1 participant overall) in participants living with HIV in study GS-US-200-4072

Baseline characteristics	GS-6207 20 mg or Placebo (*n* = 8)	GS-6207 50 mg or Placebo (*n* = 8)	GS-6207 150 mg or Placebo (*n* = 8)	GS-6207 450 mg or Placebo (*n* = 8)
Age, years, median (range)	35 (23-50)	28 (19-56)	36 (24-56)	29 (20-59)
Sex at birth: female, n (%)	1 (13)	0	1 (13)	0
Race: black, n (%)	2 (25)	2 (25)	3 (38)	3 (38)
Body mass index (kg/m^2), median (range)	25 (21-38)	25 (21-28)	26 (20-34)	25 (23-29)
HIV-1 RNA, log_{10} copies ml^{-1}, median (range)	4.47 (3.86-5.01)	4.33 (4.01-4.85)	4.57 (4.15-4.92)	4.48 (4.31-4.84)
CD4 count, cells μl^{-1}, median (range)	472 (217-574)	594 (362-1009)	388 (294-800)	430 (200-968)
ARV treatment naïve, n (%)	8 (100)	6 (75)	4 (50)	7 (88)
Median duration of follow up, Days (range) *	38 (17 to 73)	129 (122 to 136)	199 (164 to 199)	122 (113 to 136)
Safety: Preferred term				
Serious AE, n (%)				
Atrial fibrillation	0	0	0	1 (13)†
Any AE, n (%)	5 (63)	6 (75)	7 (88)	6 (75)
Injection site pain	0	4 (50)	5 (63)	4 (50)
Injection site erythema	1 (13)	1 (13)	5 (63)	2 (25)
Injection site induration	0	1 (13)	4 (50)	2 (25)

Baseline characteristics	GS-6207 20 mg or Placebo (*n* = 8)	GS-6207 50 mg or Placebo (*n* = 8)	GS-6207 150 mg or Placebo (*n* = 8)	GS-6207 450 mg or Placebo (*n* = 8)
Injection site nodule	0	1 (13)	1 (13)	2 (25)
Upper respiratory tract infection	0	0	0	4 (50)
Headache	1 (13)	0	1 (13)	1 (13)
Nausea	2 (25)	1 (13)	0	0
Oropharyngeal pain	1 (13)	1 (13)	0	1 (13)
Vomiting	2 (25)	1 (13)	0	0
Arthralgia	0	0	2 (25)	0
Constipation	0	1 (13)	0	1 (13)
Haemorrhoids	0	1 (13)	0	1 (13)
Nasopharyngitis	0	0	2 (25)	0
Rash	1 (13)	1 (13)	0	0
Syphilis	0	1 (13)	0	1 (13)

*All participants were administered the components of Biktarvy® (bictegravir/emtricitabine/tenofovir alafenamide) following 9 days of GS-6207 monotherapy.

†One participant who received either 450 mg GS-6207 or placebo experienced a serious AE of atrial fibrillation on Day 113, while receiving Biktarvy®, after amphetamine use.

Extended Data Table 9.

Clinical pharmacokinetic parameters in healthy volunteers and participants living with HIV (PLWH)

	GS-6207 in Healthy Volunteers					GS-6207 in PLWH			
Parameter	30 mg (*n* = 8)	100 mg (*n* = 8)	300 mg (*n* = 8)	450 mg (*n* = 8)	Parameter	20 mg (*n* = 6)	50 mg (*n* = 6)	150 mg (*n* = 6)	450 mg (*n* = 6)
AUC_{inf} ($hr*ng\ ml^{-1}$)	8,700 (27.1)	27,300 (41.5)	86,100 (18.3)	108,000 (24.4)	C_{D9} ($ng\ ml^{-1}$)	2.58 (41.5)	4.40 (89.9)	12.9 (39.3)	38.2 (35.1)
AUC_{last} ($hr*ng\ ml^{-1}$)	5,500 (42.2)	23,600 (45.1)	73,100 (35.4)	97,600 (29.9)	C_{D9} / $paEC_{95}$ (mean)	0.67	1.14	3.33	9.87
AUC_{exp} (%)	17.6 (69.4)	6.78 (65.0)	5.39 (126)	3.29 (69.9)					
C_{max} ($ng\ ml^{-1}$)	3.2 (39.8)	14.7 (58.4)	47.9 (27.7)	58.4 (39.2)					
T_{max} (day)	35.0 (16.5, 38.5)	21.0 (9.50, 39.0)	31.5 (14.0, 35.0)	14.0 (6.00, 31.5)					
$T_{1/2}$ (day)	37.0 (32.8, 46.2)	31.9 (21.3, 48.2)	45.4 (26.6, 62.5)	39.7 (29.7, 48.7)					

Data are shown to three significant figures and are presented as mean (%CV), except T_{max} and $t_{1/2}$: median (Q1, Q3); C_{D9} = GS-6207 plasma concentration on day 9; C_{D9} / $paEC_{95}$ = fold EC_{95} coverage on day 9.

Extended Data Table 10.

Plasma HIV-1 RNA levels and genotype in PLWH (GS-US-200-4072)

GS-6207 Dose	Participant ID	Baseline (day 0) HIV-1 RNA (log_{10} copies ml^{-1})	Maximum HIV-1 RNA change through day 9 (log_{10} copies ml^{-1})	Capsid genotype (day 9) (relative to baseline sequence)
20 mg	20-1	4.84	−0.83	wild-type
	20-2	3.86	−1.58	wild-type
	20-3	4.90	−1.74	Q67Q/H
	20-4	4.19	−1.43	wild-type
	20-5	4.21	−1.33	wild-type
	20-6	4.73	−1.21	ND
50 mg	50-1	4.01	−2.39	ND
	50-2	4.81	−1.55	wild-type
	50-3	4.3	−1.61	wild-type
	50-4	4.33	−2.32	ND
	50-5	4.85	−1.16	wild-type
	50-6	4.32	−1.73	ND
150 mg	150-1	4.61	−2.06	ND
	150-2	4.55	−1.68	wild-type
	150-3	4.58	−1.86	wild-type
	150-4	4.25	−1.49	ND
	150-5	4.61	−1.87	wild-type
	150-6	4.31	−1.62	ND
450 mg	450-1	4.31	−2.32	ND
	450-2	4.38	−2.86	ND
	450-3	4.53	−2.11	ND
	450-4	4.84	−1.83	wild-type
	450-5	4.44	−1.58	wild-type
	450-6	4.62	−2.52	ND

ND, not determined owing to repeated sequence assay failures.

Supplementary Material

Refer to Web version on PubMed Central for supplementary material.

Authors

John O. Link[1], Martin S. Rhee[1], Winston C. Tse[1,2], Jim Zheng[1], John R. Somoza[1], William Rowe[1], Rebecca Begley[1], Anna Chiu[1], Andrew Mulato[1], Derek Hansen[1], Eric Singer[1], Luong K. Tsai[1], Rujuta A. Bam[1], Chien-Hung Chou[1], Eda Canales[1], Gediminas Brizgys[1], Jennifer R. Zhang[1], Jiayao Li[1], Michael Graupe[1], Philip Morganelli[1], Qi Liu[1,3], Qiaoyin Wu[1], Randall L. Halcomb[1,4], Roland D. Saito[1,2], Scott D. Schroeder[1], Scott E. Lazerwith[1], Steven Bondy[1], Debi Jin[1], Magdeleine Hung[1], Nikolai Novikov[1], Xiaohong Liu[1], Armando G. Villaseñor[1], Carina E.

Cannizzaro[1], Eric Y. Hu[1], Robert L. Anderson[1,5], Todd C. Appleby[1], Bing Lu[1], Judy Mwangi[1], Albert Liclican[1], Anita Niedziela-Majka[1], Giuseppe A. Papalia[1], Melanie H. Wong[1], Stephanie A. Leavitt[1], Yili Xu[1], David Koditek[1], George J. Stepan[1], Helen Yu[1], Nikos Pagratis[1], Sheila Clancy[1], Shekeba Ahmadyar[1], Terrence Z. Cai[1,6], Scott Sellers[1], Scott A. Wolckenhauer[1], John Ling[1], Christian Callebaut[1], Nicolas Margot[1], Renee R. Ram[1], Ya-Pei Liu[1], Rob Hyland[1], Gary I. Sinclair[7], Peter J. Ruane[8], Gordon E. Crofoot[9], Cheryl K. McDonald[10], Diana M. Brainard[1], Latesh Lad[1], Swami Swaminathan[1], Wesley I. Sundquist[11], Roman Sakowicz[1], Anne E. Chester[1], William E. Lee[1], Eric S. Daar[12], Stephen R. Yant[1,*], Tomas Cihlar[1]

Affiliations

[1]Gilead Sciences, Foster City, CA, USA

[2]Present address: Vir Biotechnology, Inc, San Francisco, CA, USA

[3]Present address: Center for Drug Evaluation and Research, US Food and Drug Administration, Silver Spring, MD, USA

[4]Present address: Terns Pharmaceuticals, Foster City, CA, USA

[5]Present address: MyoKardia Inc, South San Francisco, CA, USA

[6]Present address: Bayer, Berkeley, CA, USA

[7]AIDS Arms Inc. DBA Prism Health North Texas, Dallas, TX, USA

[8]Ruane Clinical Research Group, Inc., Los Angeles, CA, USA

[9]The Crofoot Research Center, Inc., Houston, TX, USA

[10]Texas Centers for Infectious Disease Associates, Fort Worth, TX, USA

[11]Department of Biochemistry, University of Utah School of Medicine, Salt Lake City, UT, USA

[12]Division of HIV Medicine at Harbor-UCLA Medical Center, David Geffen School of Medicine at UCLA, Torrance, CA, USA

Acknowledgements:

We thank D. Cowfer, K. Brendza, G. Czerwieniec, M. Tsiang, K. Wang, G. Lane, M. Kenney, M. Ceo, S. Kazerani, T. Lane, L. Meng, T. Rainey, A. Vandehey, A. Wagner, M. O'Keefe, J. Yoon, S. Neville, W. Lew, B. Ross, Q. Wang, J. Cha, M. Tran and K. Nguyen for their support and contributions, and all the people who participated in the Phase I clinical trials, including the study participants, their families, and the principal investigators and their staff.

Main References

1. Grant RM, Lama JR & Anderson PL Preexposure chemoprophylaxis for HIV prevention in men who have sex with men. [Protocol]. N Engl J Med 363, 1–97 (2010). [PubMed: 20573919]
2. Baeten JM, Donnell D & Ndase P Antiretroviral prophylaxis for HIV prevention in heterosexual men and women. [Protocol]. N Engl J Med 367, 1–205 (2012). [PubMed: 22716935]
3. Molina JM et al. On-Demand Preexposure Prophylaxis in Men at High Risk for HIV-1 Infection. N Engl J Med 373, 2237–2246, doi:10.1056/NEJMoa1506273 (2015). [PubMed: 26624850]
4. Thigpen MC et al. Antiretroviral Preexposure Prophylaxis for Heterosexual HIV Transmission in Botswana [Supplementary Appendix]. N Eng J Med 367, 423–434 (2012).

5. World Health Organization (WHO). HIV/AIDS fact sheets. https://www.who.int/news-room/fact-sheets/detail/hiv-aids. 11 15 (2019).
6. Emu B et al. Phase 3 Study of Ibalizumab for Multidrug-Resistant HIV-1. N Engl J Med 379, 645–654, doi:10.1056/NEJMoa1711460 (2018). [PubMed: 30110589]
7. Bangsberg D et al. Non-adherence to highly active antiretroviral therapy predicts progression to AIDS AIDS 15, 1181–1183 (2001). [PubMed: 11416722]
8. Marrazzo JM et al. Tenofovir-based preexposure prophylaxis for HIV infection among African women. N Engl J Med 372, 509–518, doi:10.1056/NEJMoa1402269 (2015). [PubMed: 25651245]
9. Anderson PL et al. Emtricitabine-tenofovir concentrations and pre-exposure prophylaxis efficacy in men who have sex with men. Science translational medicine 4, 151ra125, doi:10.1126/scitranslmed.3004006 (2012).
10. Gulick RM & Flexner C Long-Acting HIV Drugs for Treatment and Prevention. Annu Rev Med 70, 137–150, doi:10.1146/annurev-med-041217-013717 (2019). [PubMed: 30355266]
11. Thenin-Houssier S & Valente ST HIV-1 Capsid Inhibitors as Antiretroviral Agents. Curr HIV Res 14, 270–282 (2016). [PubMed: 26957201]
12. Carnes SK, Sheehan JH & Aiken C Inhibitors of the HIV-1 capsid, a target of opportunity. Curr Opin HIV AIDS 13, 359–365, doi:10.1097/COH.0000000000000472 (2018). [PubMed: 29782334]
13. Scott DE, Bayly AR, Abell C & Skidmore J Small Molecules, Big Targets: Drug Discovery Faces the Protein-Protein Interaction Challenge. Nat Rev Drug Discov 15, 533–550, doi:10.1038/nrd.2016.29 (2016). [PubMed: 27050677]
14. Freed EO HIV-1 Assembly, Release and Maturation. Nat Rev Microbiol 13, 484–496, doi:10.1038/nrmicro3490 (2015). [PubMed: 26119571]
15. Ganser BK, Li S, Klishko VY, Finch JT & Sundquist WI Assembly and Analysis of Conical Models for the HIV-1 Core. Science 283, 80–83 (1999). [PubMed: 9872746]
16. Yamashita M & Engelman AN Capsid-Dependent Host Factors in HIV-1 Infection. Trends Microbiol 25, 741–755, doi:10.1016/j.tim.2017.04.004 (2017). [PubMed: 28528781]
17. Huang PT et al. FEZ1 Is Recruited to a Conserved Cofactor Site on Capsid to Promote HIV-1 Trafficking. Cell reports 28, 2373–2385 e2377, doi:10.1016/j.celrep.2019.07.079 (2019). [PubMed: 31422020]
18. Fernandez J et al. Transportin-1 Binds to the HIV-1 Capsid Via a Nuclear Localization Signal and Triggers Uncoating. Nat Microbiol 4, 1840–1850, doi:10.1038/s41564-019-0575-6 (2019). [PubMed: 31611641]
19. Carlson LA et al. Three-Dimensional Analysis of Budding Sites and Released Virus Suggests a Revised Model for HIV-1 Morphogenesis. Cell host & microbe 4, 592–599, doi:10.1016/j.chom.2008.10.013 (2008). [PubMed: 19064259]
20. Briggs JA, Wilk T, Welker R, Krausslich HG & Fuller SD Structural Organization of Authentic, Mature HIV-1 Virions and Cores. EMBO J 22, 1707–1715, doi:10.1093/emboj/cdg143 (2003). [PubMed: 12660176]
21. Yant SR et al. A Highly Potent Long-Acting Small-Molecule HIV-1 Capsid Inhibitor with Efficacy in a Humanized Mouse Model. Nat Med 25, 1377–1384, doi:10.1038/s41591-019-0560-x (2019). [PubMed: 31501601]
22. Graupe M et al. Therapeutic compounds. U.S. Patent 10,071,985 B2. 9 11 (2018).
23. Matreyek KA, Yucel SS, Li X & Engelman A Nucleoporin NUP153 Phenylalanine-Glycine Motifs Engage a Common Binding Pocket Within the HIV-1 Capsid Protein to Mediate Lentiviral Infectivity. PLoS pathogens 9, 1–21, doi:10.1371/journal.ppat.1003693 (2013).
24. Price AJ et al. CPSF6 Defines a Conserved Capsid Interface that Modulates HIV-1 Replication. PLoS pathogens 8, 1–14, doi:10.1371/journal.ppat.1002896 (2012).
25. Price AJ et al. Host Cofactors and Pharmacologic Ligands Share an Essential Interface in HIV-1 Capsid That Is Lost upon Disassembly. PLoS pathogens 10, 1–17, doi:10.1371/journal.ppat.1004459 (2014).
26. Bhattacharya A et al. Structural Basis of HIV-1 Capsid Recognition by PF74 and CPSF6. Proc Natl Acad Sci U S A 111, 18625–18630, doi:10.1073/pnas.1419945112 (2014). [PubMed: 25518861]

27. Lee K et al. Flexible Use of Nuclear Import Pathways by HIV-1. Cell host & microbe 7, 221–233, doi:10.1016/j.chom.2010.02.007 (2010). [PubMed: 20227665]
28. Perrier M et al. Prevalence of Gag Mutations Associated with in vitro Resistance to Capsid Inhibitor GS-CA1 in HIV-1 Antiretroviral-Naive Patients. J Antimicrob Chemother 72, 2954–2955, doi:10.1093/jac/dkx208 (2017). [PubMed: 29091184]
29. Li G et al. Functional Conservation of HIV-1 Gag: Implications for Rational Drug Design. Retrovirology 10, 126, doi:10.1186/1742-4690-10-126 (2013). [PubMed: 24176092]
30. Yant SR et al. in 10th IAS Conference on HIV Science (IAS 2019).

Methods Only References

31. Tsiang M et al. Antiviral Activity of Bictegravir (GS-9883), a Novel Potent HIV-1 Integrase Strand Transfer Inhibitor with an Improved Resistance Profile. Antimicrob Agents Chemother 60, 7086–7097, doi:10.1128/AAC.01474-16 (2016). [PubMed: 27645238]
32. Margot NA, Gibbs CS & Miller MD Phenotypic susceptibility to bevirimat in isolates from HIV-1-infected patients without prior exposure to bevirimat. Antimicrob Agents Chemother 54, 2345–2353, doi:10.1128/AAC.01784-09 (2010). [PubMed: 20308382]
33. Nakabayashi H, Taketa K, Miyano K, Yamane T & Sato J Growth of human hepatoma cells lines with differentiated functions in chemically defined medium. Cancer Res 42, 3858–3863 (1982). [PubMed: 6286115]
34. Balakrishnan M et al. Non-catalytic site HIV-1 integrase inhibitors disrupt core maturation and induce a reverse transcription block in target cells. PLoS ONE 8, e74163, doi:10.1371/journal.pone.0074163 (2013). [PubMed: 24040198]
35. Prichard MN & Shipman C Jr. Analysis of combinations of antiviral drugs and design of effective multidrug therapies. Antivir Ther 1, 9–20 (1996). [PubMed: 11322261]
36. Bam RA et al. TLR7 Agonist GS-9620 Is a Potent Inhibitor of Acute HIV-1 Infection in Human Peripheral Blood Mononuclear Cells. Antimicrob Agents Chemother 61, e01369–01316 (2017). [PubMed: 27799218]
37. Warren TK et al. Therapeutic efficacy of the small molecule GS-5734 against Ebola virus in rhesus monkeys. Nature 531, 381–385, doi:10.1038/nature17180 (2016). [PubMed: 26934220]
38. Hung M et al. Large-Scale Functional Purification of Recombinant HIV-1 Capsid. PLoS ONE 8, 1–11, doi:10.1371/journal.pone.0058035 (2013).
39. Pornillos O et al. X-ray Structures of the Hexameric Building Block of the HIV Capsid. Cell 137, 1–21, doi:10.1016/j.cell.2009.04.063 (2009).
40. Pornillos O, Ganser-Pornillos BK & Yeager M Atomic-Level Modelling of the HIV Capsid. Nature 469, 424–427, doi:10.1038/nature09640 (2011). [PubMed: 21248851]
41. Kissinger CR, Gehlhaar DK & Fogel DB Rapid automated molecular replacement by evolutionary search. Acta crystallographica. Section D, Biological crystallography 55, 484–491 (1999). [PubMed: 10089360]
42. Adams PD et al. PHENIX: a comprehensive Python-based system for macromolecular structure solution. Acta crystallographica. Section D, Biological crystallography 66, 213–221, doi:10.1107/S0907444909052925 (2010). [PubMed: 20124702]
43. Emsley P, Lohkamp B, Scott WG & Cowtan K Features and development of Coot. Acta crystallographica. Section D, Biological crystallography 66, 486–501, doi:10.1107/S0907444910007493 (2010). [PubMed: 20383002]

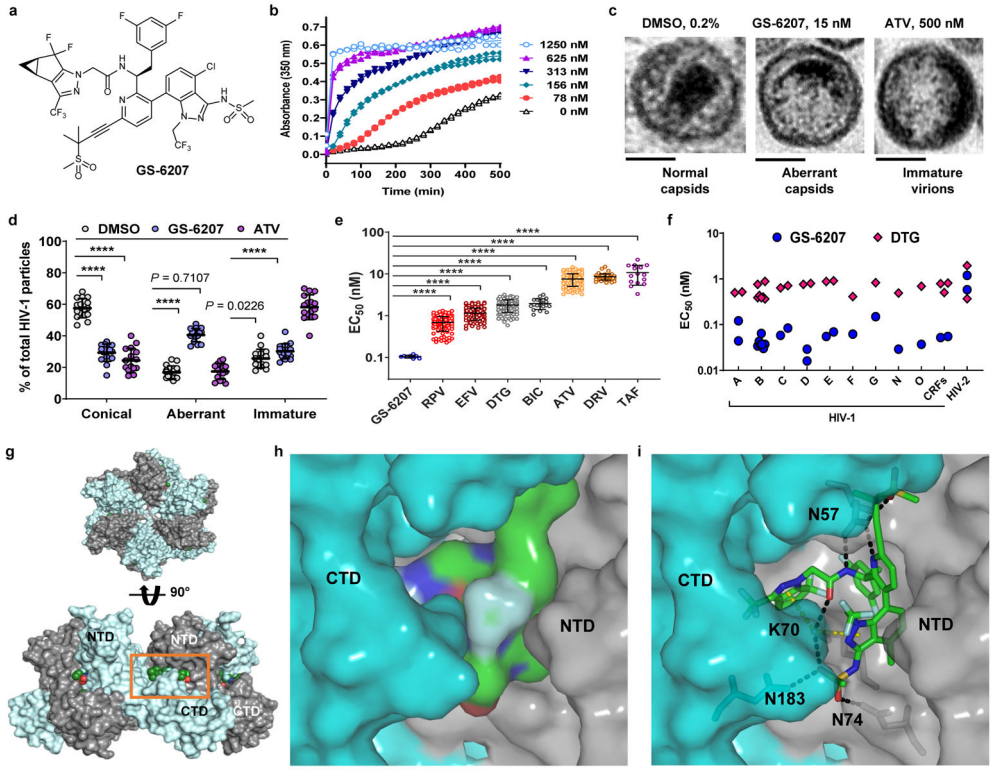

Figure 1: GS-6207 is a potent CA-targeting inhibitor of HIV replication.

a, GS-6207. **b,** Light scattering (absorbance at 350 nm) responses showing the rate and extent of in vitro CA (20 μM) assembly in 2M NaCl in the presence and absence of GS-6207. Data are representative of four independent experiments ($n = 2$ biological replicates each). **c,** Representative thin-section electron micrograph images of HIV-1 produced in the presence of 0.2% DMSO, GS-6207 or the HIV-1 protease inhibitor atazanavir (ATV). Scale bars, 50 nm. **d,** Quantitation for c. Data are mean ± s.d. from representative images of HIV-1 produced in one of two independent experiments (DMSO, $n = 737$ virions; GS-6207, $n = 591$; ATV, $n = 618$). All P values, here and throughout, by unpaired two-tailed Student's t-test with Welch's correction. ****$P < 0.0001$. **e,** Inhibition of HIV-1_{IIIb} in MT-4 cells. Data are mean ± s.d. from four biological replicates in each of 8 to 115 independent experiments: GS-6207 ($n = 8$), rilpivirine (RPV, $n = 113$), efavirenz (EFV, $n = 113$), dolutegravir (DTG, $n = 115$), bictegravir (BIC, $n = 20$), ATV ($n = 113$), darunavir (DRV, $n = 60$), and tenofovir alafenamide (TAF, $n = 15$). ****$P < 1 \times 10^{-15}$. **f,** Inhibition of HIV-2 and HIV-1 Group M (subtypes A-G, CRFs), N and O clinical isolates. Data represent individual isolates ($n = 3$ biological replicates each). CRFs, circulating recombinant forms. **g,** X-ray crystal structure of GS-6207-CA hexamer complex. Top and side views of CA hexamer (individual CA monomers colored cyan and gray). The GS-6207 binding site, located between the NTD of one CA monomer and the CTD of an adjacent monomer, is boxed. **h,** Space-filling view of GS-6207 in its binding site (X-ray structure). **i,** Hydrogen bonds (dashed black lines, $n = 7$) and cation-π interactions (dashed yellow lines, $n = 2$) are shown between GS-6207 and CA residues.

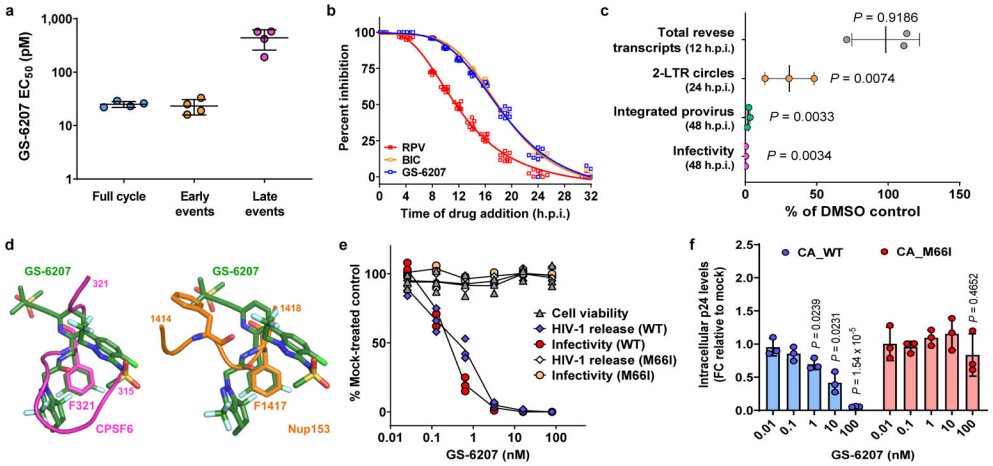

Figure 2: GS-6207 inhibits multiple capsid-dependent HIV-1 replication steps.

a, Antiviral activity of GS-6207 throughout a full replication cycle or when selectively present during target cell infection (early events) or virus production (late events). Data are mean ± s.d. from four independent experiments (n = 3 biological replicates each). **b,** Time-of-addition study indicating when GS-6207 inhibits HIV-1 replication relative to rilpivirine (RT inhibitor) and bictegravir (IN inhibitor). Data are means from one of two representative independent experiments (n = 8 biological replicates per group in each experiment). **c,** Effect of GS-6207 (1.25 nM) on the intracellular abundance of various HIV-1 DNA forms. Data are mean ± s.d. from one of two representative independent experiments (n = 3 biological replicates each). **d,** Overlay of GS-6207 with CA-binding peptides from nuclear import factors CPSF6 and Nup153 (ref. 25) in their shared binding pocket. **e,** Effect of GS-6207 on HEK293T producer cell viability, HIV-1 particle production and infectivity. Data are means from one of three representative independent experiments (n = 3 biological replicates each). M66I, GS-6207 resistance-associated CA binding site variant. **f,** Effect of GS-6207 on intracellular CA levels. Data are mean ± s.d. from three independent experiments (n = 3 biological replicates each). For gel source data, see Supplementary Figure 1.

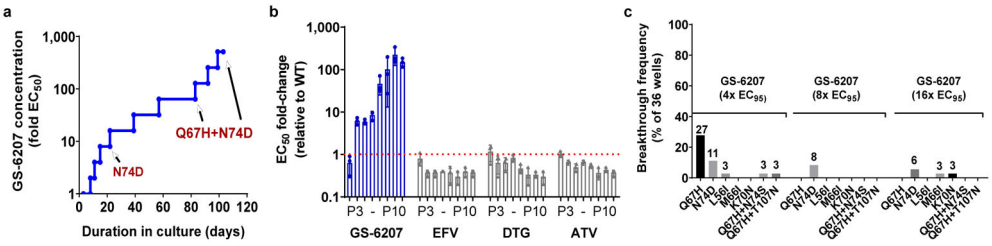

Figure 3: Resistance to GS-6207 maps to CA.

a, Emergent CA substitutions denoted during resistance selection in HIV-1_{HXB2D}-infected MT-2 cells by GS-6207 dose-escalation. Data are representative of one of two biological replicates from a single selection experiment. **b,** Fold resistance of GS-6207-selected viral isolate passage 3 to 10 (P3 – P10) to GS-6207 and control antiretrovirals. Data are mean ± s.d. from three independent experiments (n = 3 biological replicates each). Red dotted line defines the cut-off for drug resistance. WT, wild-type HIV-1; EFV, efavirenz; DTG, dolutegravir; ATV, atazanavir. **c,** Frequency of GS-6207-selected CA variants observed at fixed GS-6207 concentrations in PBMCs infected with clinical HIV-1 isolates.

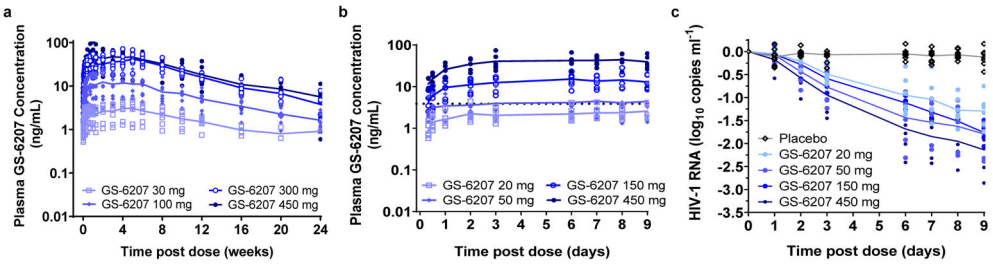

Figure 4: Clinical testing of GS-6207 in humans.

a, Mean plasma concentration-time profile of GS-6207 after a single subcutaneous administration of 30-450 mg of drug to uninfected participants (n = 8 within each dosing arm). **b,** Mean plasma concentration-time profile of GS-6207 after a single subcutaneous administration of 20-450 mg to HIV-infected participants (n = 6 within each dosing arm). Red dotted line defines $paEC_{95}$ for GS-6207. **c,** Mean log_{10} change in plasma HIV-1 RNA after a single subcutaneous administration of 20-450 mg GS-6207 to eight participants with untreated HIV-1 infection randomized to drug (n = 6) or placebo (n = 2) within each dosing arm.